Applied Catalysis B: Environmental 132–133 (2013) 452–459

Contents lists available at SciVerse ScienceDirect

Applied Catalysis B: Environmental

journal homepage: www.elsevier.com/locate/apcatb

One-step synthesis of easy-recycling TiO_2-rGO nanocomposite photocatalysts with enhanced photocatalytic activity

Ping Wang[a], Jin Wang[a], Xuefei Wang[a], Huogen Yu[a,*], Jiaguo Yu[b], Ming Lei[c,*], Yonggang Wang[c]

[a] Department of Chemistry, School of Science, Wuhan University of Technology, Wuhan 430070, PR China
[b] State Key Laboratory of Advanced Technology for Material Synthesis and Processing, Wuhan University of Technology, Wuhan 430070, PR China
[c] School of Science, Beijing University of Posts and Telecommunications, Beijing 100876, PR China

ARTICLE INFO

Article history:
Received 25 October 2012
Received in revised form 8 December 2012
Accepted 9 December 2012
Available online 20 December 2012

Keywords:
Reduced graphene oxide
TiO_2
Photocatalytic activity
Easy recycling
Green method

ABSTRACT

The addition of reduced graphene oxide (rGO) in the TiO_2 has been demonstrated to be one of the effective methods to improve the photocatalytic performance of TiO_2 photocatalyst. Despite tremendous efforts, developing facile and green synthetic method of TiO_2-rGO nanocomposites still remains a great challenge. In this study, a one-step green hydrothermal method for the fabrication of easily recycled TiO_2-rGO composites, based on the initial formation of strong-coupling TiO_2-GO nanocomposite and the subsequent in situ reduction of GO to rGO during hydrothermal treatment, was developed in the pure water without using any reductant and surfactant. It is found that the TiO_2 nanoparticles with a clean surface and a good dispersion are highly required for the formation of the easy-recycling TiO_2-rGO composite photocatalyst. Photocatalytic experimental results indicated that compared with the high-efficiency P25 TiO_2 precursor, the photocatalytic performance could be obviously improved (about 23%) for the decomposition of phenol after coupling 1-wt% rGO. The enhanced photocatalytic performance can be attributed the cooperation effect of the effective separation of charge carriers via rGO cocatalyst, the enrichment of phenol molecular on the rGO, and the strong coupling interaction between TiO_2 nanoparticles and rGO nanosheets. Considering its completely green and facile preparation and recyclable feature from an aqueous solution, the present TiO_2-rGO nanocomposite photocatalyst can be regards as one of the ideal photocatalysts for various potential applications.

1. Introduction

TiO_2 is one of the most widely investigated photocatalysts that exhibits effective photocatalytic degradation for various organic pollutants [1–3]. However, the TiO_2 photocatalyst still cannot be widely used in practical applications due to its low photocatalytic activity. Therefore, it is highly required to develop new methods to improve the photocatalytic performance of TiO_2 photocatalyst. Compared with a single-component photocatalyst, composite photocatalysts usually exhibit a higher photocatalytic performance. The general principle for the enhanced photocatalytic performance of these composite photocatalysts is that they have different electronic energy levels so that the charge separation can be enhanced by the internal electric field driving force [4,5]. Various strategies have been developed to synthesize TiO_2 composite materials for the inhibition of high electron-hole recombination rate, such as coupling with noble metal [6,7], transition metal ions (or their oxides) [8,9] and other semiconductors [10,11]. Recently, the addition of graphene has been demonstrated to be one of the effective methods to improve the photocatalytic performance of TiO_2 owing to its large specific surface area and excellent mobility of charge carriers [12–15].

Graphene oxide (GO) is one of the main precursors for the preparation of various graphene-based photocatalytic materials due to its large-scale production and facile synthetic method [16]. However, the microstructures of the GO are completely different from that of the pristine graphene owing to the presence of large amount of oxygen-containing functional groups such as hydroxyl and epoxide, resulting in a great decrease of the electronic properties [17,18]. Therefore, for the preparation of highly efficient graphene-based TiO_2 photocatalysts, the deoxygenation/reduction process of GO is highly required in order to recover its excellent mobility of charge carriers. It was reported that hydrazine and sodium borohydride have been demonstrated to be excellent reducing agents for the effective reduction of GO [19,20]. However, considering their toxic affect on both human and environmental health, the exploration of greener and more sustainable reduced strategy of GO would be greatly beneficial for the preparation of TiO_2-rGO photocatalysts. Several researcher groups have reported that UV-light photocatalytic reduction of the GO is an effective and green method

* Corresponding authors. Tel.: +86 27 87871029; fax: +86 27 87879468.
E-mail addresses: yuhuogen@yahoo.cn (H. Yu), mlei@bupt.edu.cn (M. Lei).

0926-3373/$ – see front matter © 2012 Elsevier B.V. All rights reserved.
http://dx.doi.org/10.1016/j.apcatb.2012.12.009

for the preparation of TiO_2-rGO composites [16,21]. In addition, hydrothermal/solvothermal route has been demonstrated to be an efficient method for the GO reduction to obtain the TiO_2-rGO composites [22–26]. However, various additives (alkaline, ethanol, acid, etc.) [22,23] and Ti precursors ($TiCl_4$, $TiCl_3$, $Ti(OC_4H_9)_4$, TiF_4, etc.) [23–26] have been widely used in the hydrothermal/solvothermal processes. Owing to the severe aggregation of the rGO and the toxicity problems of many starting materials for TiO_2 nanoparticles, developing a facile and green synthetic method of the TiO_2-rGO composites still remains a great challenge. In addition, the present reported studies about the TiO_2-rGO composites are mainly focused on the reduction of GO, and seldom researchers have paid their attention on the enhanced coupling interaction between the TiO_2 and rGO nanosheets [22–26]. Considering the importance of charge carrier transfer between the TiO_2 and rGO for the enhanced photocatalytic performance, it is very necessary and important to control their interface interaction in order to prepare highly efficient TiO_2-rGO photocatalyst.

Compared with the usual powered photocatalysts, the easily recyclable photocatalysts have more advantages in the water treatment and purification systems [27,28]. In this study, the easy-recycling TiO_2-rGO composite with a strong coupling interface was prepared by a green one-step hydrothermal method in a pure water system without using any reducing agents and additives. The one-step formation mechanism of the strong-coupling TiO_2-rGO composites is based on the initial formation of strong-coupling TiO_2-GO nanocomposite and the subsequent in situ reduction of GO to rGO during hydrothermal treatment. The photocatalytic activity of the TiO_2-rGO composites was evaluated by the degradation of phenol under UV irradiation. To the best of our knowledge, this is the first report about the one-step green hydrothermal preparation of the easy-recycling TiO_2-rGO composite photocatalysts. Considering the facile and completely green preparation of the TiO_2-rGO composite photocatalysts, this work may provide some insight into the design of other novel graphene-based materials, and the present recoverable TiO_2-rGO composite photocatalysts can be regarded as one of the ideal photocatalysts for the various potential applications.

2. Experimental

Commercial P25 TiO_2 power was obtained from Degussa and used as the TiO_2 precursor, and all the other reagents (analytical grade) were supplied by Shanghai Chemical Reagent Ltd. (PR China) and used as received without further purification.

2.1. Synthesis of GO

The graphene oxide was synthesized from natural graphite powder (99.95%) [29]. Briefly, 3 g of graphite, 2.5 g of $K_2S_2O_8$ and 2.5 g of P_2O_5 were added into 12 ml of concentrated H_2SO_4 under strong stirring at 80 °C for 4.5 h. After the solution was cooled down to room temperature naturally, 0.5 L of deionized (DI) water was added into the above solution and aged for 12 h. The suspension was filtered, washed and dried to obtain the black solid. The black solid was mixed with 120 ml of concentrated H_2SO_4 and 15 g of $KMnO_4$ in an ice bath below 20 °C, and then was transferred to a water bath and magnetically stirred at 35 °C for 2 h. The resulted dark-brown paste was diluted with the slow addition of 250 ml of DI water and then stirred for another 2 h. A 20 mL (30 wt%) of H_2O_2 was slowly added to quench the solution to produce a golden-brown solution. After the resultant product was centrifuged, the sample was washed with HCl (1:10) and DI water, respectively, until the pH of the washed solution was ca. 6. Finally, the product was dried at 40 °C in vacuum to obtain the GO sample.

The GO (0.05%) solution was obtained by ultrasonic dispersion of GO (0.5 g) in DI water (1 L) for 2 h.

2.2. Synthesis of the easy-recycling TiO_2-rGO nanocomposite

Before the synthesis of TiO_2-rGO nanocomposite, the P25 TiO_2 precursor was pre-treated at 550 °C for 2 h in order to obtain a clean TiO_2 surface after the removal of surface adsorbed substances. The TiO_2-rGO composite was obtained via one-step hydrothermal method. In brief, 0.5 g of TiO_2 was first added to the calculated amount of GO solution. After stirring for 2 h, the mixing solution was transferred into a 100 ml of Teflon-sealed autoclave and maintained at 150 °C for 5 h. The resulting composite was recovered by centrifugation, rinsed with DI water for several times, and fully dried in vacuum at 60 °C for 12 h. The amount of graphene in the TiO_2-graphene composites was controlled to be 0, 0.05, 1, and 5 wt%, and the corresponding samples were denoted as TiO_2, TiO_2-rGO (0.05 wt%), TiO_2-rGO (1 wt%), and TiO_2-rGO (5 wt%), respectively. For comparison, the GO solution was also hydrothermally treated at 150 °C for 5 h and the resulted sample was denoted as rGO.

For comparison, the lab-made TiO_2 nanoparticles were also used as the TiO_2 precursor for the preparation of TiO_2-rGO composite. The lab-made TiO_2 nanoparticles was prepared from the hydrolysis of tetrabutyl titanate and then calcined at 500 °C for 2 h, as shown in our previous study [30]. The resulted lab-made TiO_2 nanoparticles show an aggregate with a size of 100–500 nm and a specific surface area of 96.1 m^2/g [30].

2.3. Characterization

X-ray diffraction (XRD) patterns were obtained on a D/MAX-RBX-ray diffractometer (Rigaku, Japan). X-ray photoelectron spectroscopy (XPS) measurements were done on a KRATOA XSAM800 XPS system with Mg Kα source. All the binding energies were referenced to the C1s peak at 284.8 eV for the surface adventitious carbon. Morphological analysis was performed with an S-4800 field emission scanning electron microscope (FESEM) (Hitachi, Japan) with an acceleration voltage of 10 kV. Raman spectra were collected using an INVIA spectrophotometer (Renishaw, UK). Fourier Transform Infrared spectra (FTIR) were acquired using a Nexus FT-IR spectrophotometer (Thermo Nicolet, America). UV–vis absorption spectra were obtained using a UV–visible spectrophotometer (UV-2550, SHI-MADZU, Japan).

2.4. Photocatalytic activity

The evaluation of photocatalytic activity of the prepared samples for the photocatalytic decomposition of phenol aqueous solution was performed at ambient temperature [31–33]. Experimental details were shown as follows: 50 mg of the sample was dispersed into 10 ml of phenol solution (10 mg L^{-1}) in a disk with a diameter of ca. 5 cm. The mixed suspension was placed in dark for 2 h to reach the adsorption-desorption equilibrium between the photocatalyst and phenol before irradiation. The integrated UV intensity in the range of 310–400 nm striking the sample, measured with a UV radiometer (Model: UV-A, made in Photoelectric Instrument Factory of Beijing Normal University), was 2.5 mW/cm^2 with a peak wavelength of 365 nm. The concentration of phenol was determined by an UV–visible spectrophotometer (UV-1240, SHIMADZU, Japan). After light irradiation for some time, the reaction solution was centrifuged to measure the concentration of phenol. As for the phenol aqueous solution with low concentration, its photocatalytic decolorization is a pseudo-first-order reaction and its kinetics may be expressed as $\ln(c/c_0) = -kt$, where k is the apparent rate constant, and c_0 and c are the phenol concentrations at initial state and

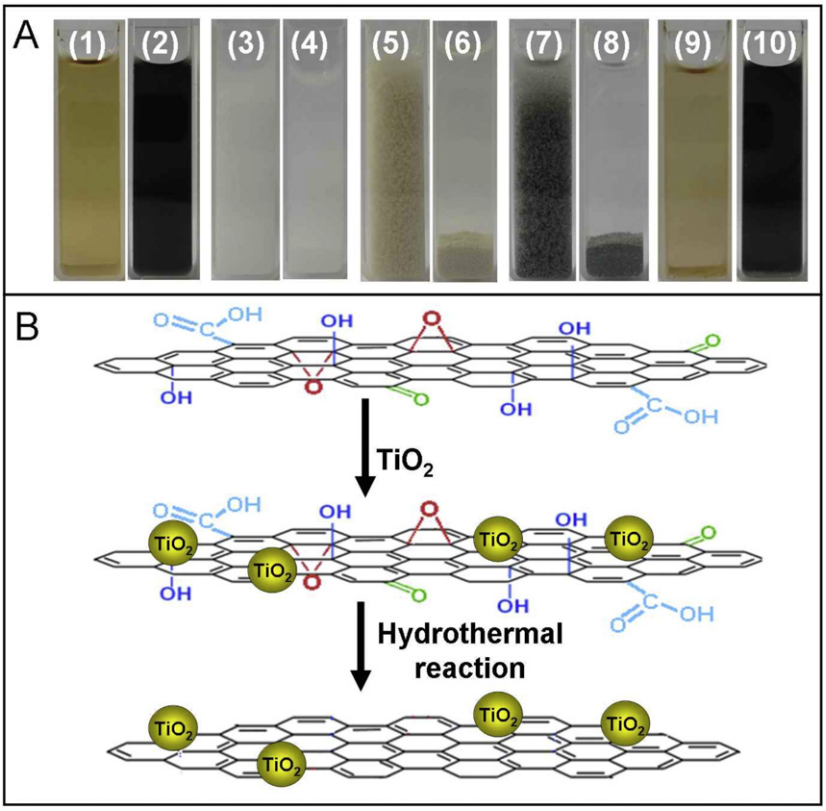

Fig. 1. (A) the photographs of various samples: (1,2) GO solution before (1) and after (2) hydrothermal treatment; (3,4) P25 TiO_2 suspension before (3) and after (4) aging for 5 min; (5,6) TiO_2-GO suspension before (5) and after (6) aging for 5 min; (7,8) hydrothermally treated TiO_2-GO suspension before (7) and after (8) aging for 5 min; (9,10) lab-made TiO_2-GO suspension before (9) and after (10) hydrothermal treatment; (B) graphical illustration for the synthesis of easy-recycling TiO_2-rGO nanocomposite.

after irradiation for t min, respectively [33]. The adsorption performance for the phenol of various photocatalysts was measured by using $(c_0 - c_a)/c_a$, where the c_0 and c_a are the phenol concentrations at initial state and after adsorption-desorption equilibrium, respectively.

3. Results and discussion

3.1. Synthesis strategy

It is well known that the GO can be well dispersed into water to form a homogeneous and stable solution owing to the presence of a lot of oxygen-containing groups such as —OH, C═O, C—O—C, and —COOH. The color of as-prepared GO solution is light yellow (Fig. 1A-1), in good agreement with the reported results [16]. After hydrothermal treatment, the color of the GO nanosheets changed obviously from light yellow to dark (Fig. 1A-2), indicating the effective reduction of GO to rGO [34–38]. Compared with the well-known reduction of GO by hydrazine or sodium borohydride, in this study, it is obviously different for the hydrothermal reduction mechanism owing to the absence of reducing agents. With increasing temperature and pressure, the physiochemical properties of water can be greatly changed, and the supercritical water becomes a fluid with unique properties such as strong electrolytic solvent power, high diffusion coefficient and ion molecules [39]. In addition, the supercritical water can exhibit strong reducing power during hydrothermal reaction, resulting in the cleavage reactions of various heterolytic bonds [39]. As a consequence, the hydrothermal method has been extensively used to prepare carbon-based nanostructures via the deoxygenation reaction of carbohydrates [40,41]. Therefore, the hydrothermal reduction mechanism of GO nanosheets in this study can be attributed to the deoxygenation/dehydration reaction of GO.

Commercial P25 TiO_2 nanoparticles, a well-known photocatalyst, usually have a good dispersion in the aqueous solution. When the P25 TiO_2 nanoparticles were dispersed into the water, a colloid suspension was obtained even after aging for 5 min owing to its small nanoparticles and good dispersion (Fig. 1A-3 and 4). However, when the P25 TiO_2 power was added into the above GO solution, a homogeneous and stable TiO_2-GO suspension was formed and the white color of the TiO_2 changed into light yellow owing to its surface coupling with GO nanosheets (Fig. 1A-5). After aging for 5 min without stirring, it is interesting to find that the TiO_2-GO composite shows a cotton-like suspension (Fig. 1A-6), completely different from the P25 TiO_2 colloid suspension (Fig. 1A-4), clear GO solution (Fig. 1A-1), and lab-made TiO_2-GO sample (Fig. 1A-9). Further observation indicates that after the precipitation of the TiO_2-GO composite, the resident solution is very clear and colorless (Fig. 1A-6), suggesting that the GO nanosheets in the solution are completely coupled on the surface of TiO_2 nanoparticles to form a TiO_2-GO composite. Additional experiment suggests that the GO nanosheets cannot be detached from the TiO_2 nanoparticles by strong stirring or ultrasonic dispersion, suggesting that there is a strong interaction between the GO nanosheets and the TiO_2 nanoparticles. Considering the excellent hydrophilicity of both GO nanosheets and the calcined TiO_2 nanoparticles, the interaction between TiO_2 nanoparticles and GO nanosheets is much higher than that of TiO_2 nanoparticles with H_2O molecules. In addition, owing to a clean surface of the P25 TiO_2 nanoparticles after the removal of various adsorbed substances via high-temperature calcination (550 °C), it is possible that the high adsorption property of TiO_2 nanoparticles also contribute their enhanced interaction with the GO nanosheets. After hydrothermal treatment at 150 °C,

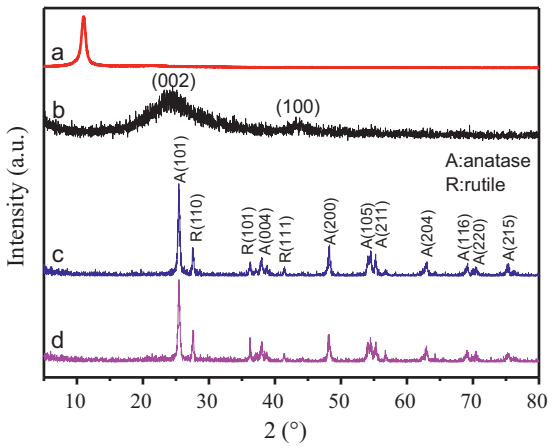

Fig. 2. XRD patterns of the (a) GO, (b) rGO, (c) TiO_2 and (d) TiO_2-rGO (1 wt%).

the color of the TiO_2-GO suspension changed obviously into black (Fig. 1A-7) due to the in situ reduction of GO. Simultaneously, the TiO_2-rGO composite with a cotton-like structure can be well maintained after hydrothermal process, which can be regarded as an ideal and novel photocatalyst with many advantages for the decomposition of organic substances in the aqueous solution (see below). In addition, the colorless upper solution after the TiO_2-rGO precipitation (Fig. 1A-8) further demonstrates the strong interaction between rGO nanosheets and the TiO_2 nanoparticles after hydrothermal process. Therefore, the one-step formation process of the suspensible TiO_2-rGO nanocomposites is based on the initial formation of strong-coupling TiO_2-GO nanocomposite and the subsequent in situ reduction of GO to rGO during hydrothermal treatment, as shown in Fig. 1B.

For the successful preparation of suspensible TiO_2-rGO composite, the effective coupling of TiO_2 nanoparticles on the GO nanosheets before hydrothermal treatment is highly required. Additional experiments indicated that when the lab-made TiO_2 nanoparticles were added into the GO solution under an identical experimental condition, no homogeneous suspension solution but a rapid precipitation of the TiO_2 sample was observed (Fig. 1A-9), though the lab-made TiO_2 nanoparticles have a higher specific surface area (S_{BET} = 96.1 m^2/g) [30] than the P25 TiO_2 samples (S_{BET} = 49.3 m^2/g) [42]. The possible reason is that the lab-made TiO_2 sample shows poorer dispersion ability in water owing to the formation of large TiO_2 aggregates with a size of 100–500 nm [30]. In addition, compared with the P25 TiO_2 sample (Fig. 1A-6), the resultant aqueous solution still shows a light-yellow color after the precipitation of TiO_2 nanoparticles (Fig. 1A-9), indicating that most of the GO nanosheets cannot be effectively coupled with the TiO_2 nanoparticles owing to smaller aggregated pores in the lab-made TiO_2 sample [30]. As a consequence, the uncoupled GO nanosheets are in situ transformed into rGO and then suspended in the solution to form black rGO solution after hydrothermal treatment (Fig. 1A-10).

3.2. Morphology and microstructures

The effective reduction of GO to rGO and successful preparation of the TiO_2-rGO composite photocatalysts via hydrothermal method can be further demonstrated by the following various technologies. It is clear that the GO usually shows a characteristic diffraction peak at 2θ = 11.0 (Fig. 2a) and a crumpled morphology (Fig. 3a) [43]. After hydrothermal treatment of the GO nanosheets, a new and wide diffraction peak (ca. 24.1°) belonging to rGO is clearly observed owing to the reduction of GO (Fig. 2b), indicating that the hydrothermal treatment is an effective method for the reduction of GO to rGO [26,43]. Therefore, when the P25 TiO_2 nanoparticles were dispersed into the GO solution and then hydrothermally treated, the obtained sample can be ascribed to the TiO_2-rGO nanocomposite (Fig. 3d). However, compared with the pure TiO_2 sample (Fig. 2c), no diffraction peak of rGO can be observed, which is due to its limited amount in the TiO_2-rGO composites. Considering the high-efficiency network structure and the well coupling interaction of rGO nanosheets and TiO_2 nanoparticles (Fig. 3c), it is expected that the suspensible TiO_2-rGO composite photocatalyst can show a high photocatalytic activity.

Fig. 4 shows the FTIR spectra of GO, rGO, TiO_2 and TiO_2-rGO samples. It is clear that the GO (Fig. 4a) shows many strong

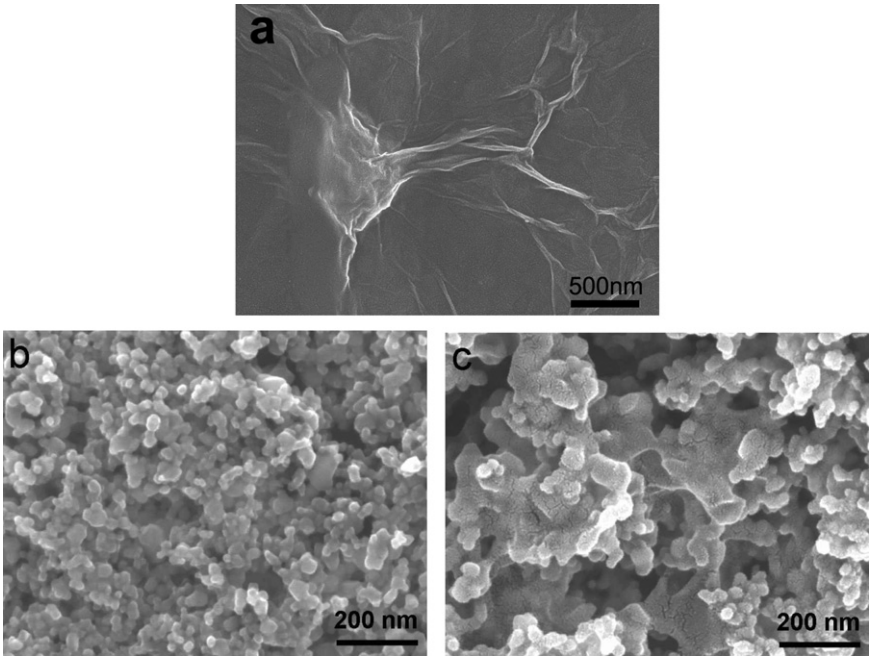

Fig. 3. FESEM images of the (a) GO, (b) TiO_2 and (c) TiO_2-rGO (1 wt%).

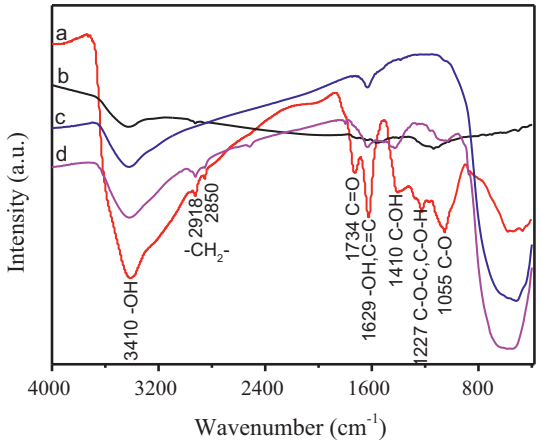

Fig. 4. FTIR spectra of the (a) GO, (b) rGO, (c) TiO_2 and (d) TiO_2-rGO (1 wt%).

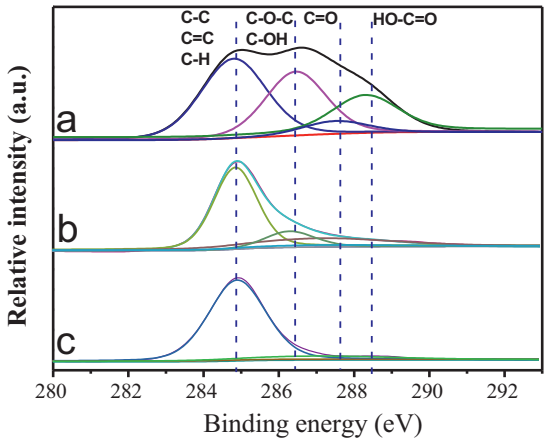

Fig. 6. XPS spectra of C 1s in the (a) GO, (b) rGO and (c) TiO_2-rGO (1 wt%).

absorption peaks that correspond to various oxygen functional groups, such as, water —OH stretching (3410 cm^{-1}), carboxylates or ketones C=O stretching (1734 cm^{-1}), water —OH bending and C=C stretching (1629 cm^{-1}), alcoholic C—OH bending (1420 cm^{-1}), epoxide C—O—C or phenolic C—O—H stretching (1227 cm^{-1}) and C-O stretching (1055 cm^{-1}) [44,45]. After hydrothermal treatment of the GO, the intensity of all absorption peaks corresponding to oxygen functional groups (C=O, C—OH, C—O—C, C—O—H and C—O) has a significant decrease (Fig. 4b), which further demonstrates the effective reduction of GO to rGO by hydrothermal method, in good agreement with the XRD results (Fig. 2). For the TiO_2 nanoparticles (Fig. 4c), the absorption peaks at 3410 cm^{-1} and 1629 cm^{-1} come from the water —OH group, while the wide peaks at 400–900 cm^{-1} is attributed to the stretching vibration of Ti—O—Ti bonds in crystalline TiO_2 [46]. After hydrothermal treatment of the TiO_2-GO suspension, the resulted TiO_2-rGO composite (Fig. 4d) shows a low absorption-peak intensity of the oxygen functional groups at 1000–1800 cm^{-1}, similar to the rGO (Fig. 4c). In addition, the strong peaks at 400–900 cm^{-1} of TiO_2-rGO composite are attributed to the stretching vibration of Ti—O—Ti and the possible Ti—O—C bonds. Therefore, the above results further confirmed the reduction of GO and the successful preparation of chemical-coupling TiO_2-rGO composite.

Raman spectroscopy can provide further information about the formation of TiO_2-rGO composite, as shown in Fig. 5. It is clear that P25 TiO_2 shows strong Raman characteristic peaks at 144 cm^{-1} ($E_{g(1)}$), 395 cm^{-1} (B_{1g}), 516 cm^{-1} (A_{1g}), and 639 cm^{-1} ($E_{g(2)}$) (Fig. 5a) [47]. After the coupling of TiO_2 nanoparticles by rGO (Fig. 5d), the intensities of the four characteristic peaks show a significant

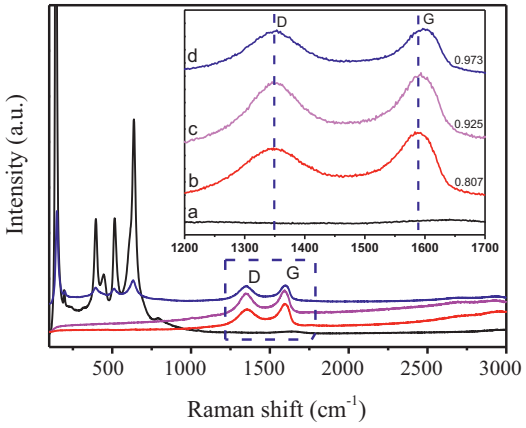

Fig. 5. Raman spectra of the (a) TiO_2, (b) GO, (c) rGO and (d) TiO_2-rGO (1 wt%).

decrease. The reason can be attributed to the fact that the surface of TiO_2 nanoparticles is homogeneously wrapped by rGO (Fig. 3c). In addition, Raman spectroscopy is also a powerful and widely used method for the characterization of sp^2 and sp^3 hybridized carbon atoms in graphene to distinguish the order and disorder/defect structures [45,48]. The characteristic Raman peaks of GO, rGO and TiO_2-rGO are shown in the inset of Fig. 5. The G band corresponds to the first-order scattering of the E_{2g} mode observed for sp^2 carbon domains, while the D band is attributed to a breathing mode of κ-point phonons of A_{1g} symmetry, which is a common feature of sp^3 defects in carbon and usually can be associated with the structural defects, amorphous carbon, or edges that break the symmetry and selection rule [48]. Therefore, the intensity ratio of the D band to the G band is usually a measure of the disorder/defects in graphene, and a smaller intensity ratio of I_D/I_G can be assigned to less sp^3 defects/disorders and larger average size (or less amount) of the in-plane graphitic crystallite sp^2 domains [48,49]. Compared with the GO (0.807), the rGO shows a higher I_D/I_G ratio (0.925), indicating that the rGO prepared by the hydrothermal method contains more defects. Considering a hydrothermal deoxygenation/reduction process, it is clear that the defects in the GO nanosheets cannot be well repaired by hydrothermal treatment and are still remained after the removal of oxygen moieties. However, compared to the dramatically increased I_D/I_G ratio of the rGO prepared from the hydrazine monohydrate, the increased number of sp^3 defects caused by the hydrothermal method is still very limited, in good agreement with the previous reports [39,49]. For the TiO_2-rGO composite, the I_D/I_G ratio is further improved to 0.973, suggesting the formation of more sp^3 defects in carbon. The possible reason for the increased sp^3 defects can be attributed to the strong interaction (such as the Ti—O—C bond) between the interface of TiO_2 nanoparticles and rGO nanosheets.

After hydrothermal reaction of GO nanosheets, the chemical state of the carbon atoms in the hexagonal lattice of graphene was changed significantly owing to the deoxygenation reaction, which can be well illustrated by the XPS results (Fig. 6). The C 1s XPS spectrum of the GO nanosheets (Fig. 6a) clearly shows the presence of four types of carbon bonds, that is, the non-oxygenated ring C (284.9 eV, including C—C, C=C, and C—H), the C—O in C—O—C or C-OH groups (286.6 eV), the carbonyl C in C=O (287.6 eV) and the carboxylate carbon in O=C—OH (288.3 eV), suggesting a considerable degree of oxidation for the GO nanosheets [50]. After hydrothermal treatment of the GO, the XPS peak intensity of these carbon–oxygen species in the resulted rGO (Fig. 6b) shows a dramatic decrease, suggesting the effective deoxygenation of GO nanosheets. Considering an identical experimental condition for the preparation of TiO_2-rGO composite, it is clear that the GO in the

Table 1
Peak area (A) ratios of oxygen-containing bonds to total area according to the XPS results.

Sample	A_{C-C}/A	A_{C-O}/A	$A_{C=O}/A$	A_{COOH}/A
GO	0.42	0.32	0.07	0.19
rGO	0.72	0.20	0.05	0.03
TiO_2-rGO (1 wt %)	0.86	0.10	0.04	0

TiO_2-GO system can be in situ reduced to form TiO_2-rGO composite (Fig. 6c). To further illustrate the hydrothermal reduction degree of the GO nanosheets, the peak area ratios of oxygen-containing bonds to total area are calculated on the basis of XPS results and the corresponding results are shown in Table 1. It is clear that the amount of oxygen-containing groups such as C—O, C═O and COOH has a significant decrease, which further provides strong evidence for the reduction of GO in TiO_2-rGO composites.

Fig. 7 shows the UV–vis spectra of the TiO_2-rGO composites. Compared with the P25 TiO_2 nanoparticles, the prepared TiO_2-rGO composite shows an obviously improved UV light absorption. Moreover, the absorption edge of the TiO_2-rGO composites shows a slight red-shift to higher wavelength, probably due to the formation of Ti—O—C bonds between the interface of TiO_2 and rGO [51,52]. With increasing amount of the rGO, the TiO_2-rGO composites show a continuously enhanced visible-light absorption in the range of 400–800 nm, which is in agreement with the color change from white to black, as shown in the inset of Fig. 7.

3.3. Photocatalytic performance

The photocatalytic performance of the TiO_2 and TiO_2-rGO composites was evaluated by the photocatalytic decomposition of phenol aqueous solution, as shown in Fig. 8A. It is clear that the commercial P25 TiO_2 shows a high photocatalytic activity ($k = 0.0039\ min^{-1}$) for the decomposition of phenol solution owing to its well-known performance for various photocatalytic reaction. After the P25 TiO_2 is coupled with 0.05-wt% rGO nanosheets, the resultant TiO_2-rGO composite shows a remarkably enhanced photocatalytic activity. Especially, when the amount of rGO increases to ca. 1 wt%, the photocatalytic performance of the P25 TiO_2 can be further improved by a factor of 23% ($k = 0.0048\ min^{-1}$). To investigate the performance stability of TiO_2-rGO composite, we repeated the photocatalytic decomposition of phenol solution five times and the corresponding results are shown in Fig. 8B. It is found that both of the TiO_2-rGO and P25 TiO_2 samples can maintain a stable and efficient photocatalytic performance, although there is a slight decrease compared with the first-cycle result. However, it should be noted that the TiO_2-rGO composite clearly shows a higher photocatalytic activity than the corresponding TiO_2 sample during repeating photocatalytic tests. With further increase of the graphene content to 5 wt%, the photocatalytic activity of the TiO_2-rGO composites has a drastic decrease, even lower than that of pure P25 TiO_2. The possible reason can be ascribed to the increase in the opacity and light scattering of TiO_2-rGO composite, and high graphene load shielding the TiO_2 from absorbing UV light, resulting in rapid decrease of irradiation passing through the reaction suspension solution [51,53].

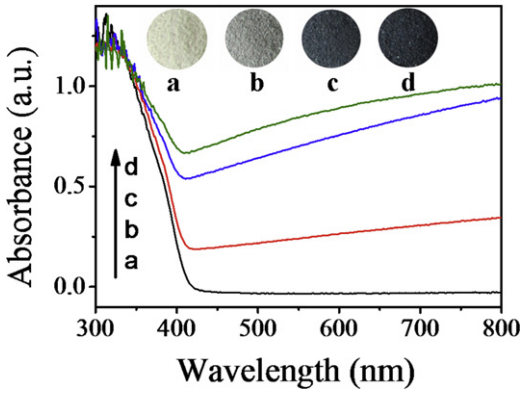

Fig. 7. UV-vis spectra of the (a) TiO_2, (b) TiO_2-rGO (0.05 wt%), (c) TiO_2-rGO (1 wt%) and (d) TiO_2-rGO (5 wt%).

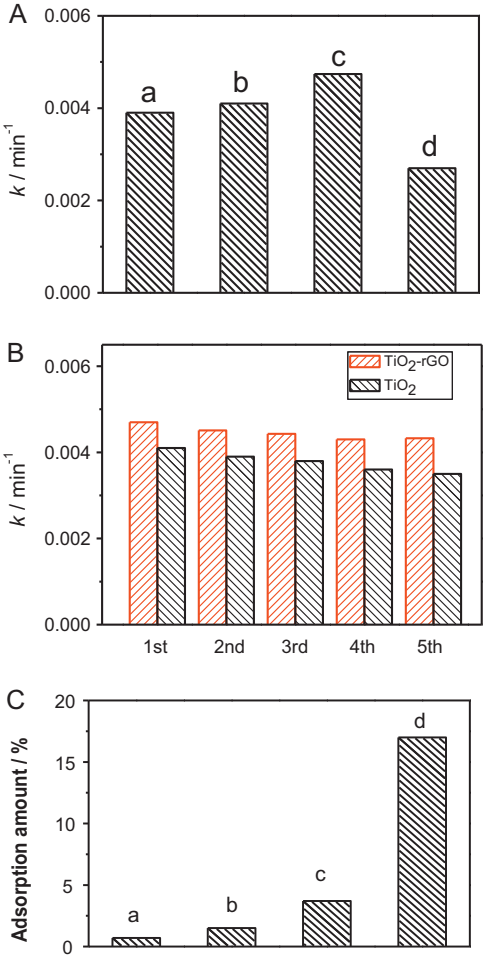

Fig. 8. (A) The rate constant (k) of the phenol decomposition by various photocatalysts; (B) the repeated photocatalytic performance of samples (a) and (c); and (C) the adsorption ability of various photocatalysts for phenol: (a) TiO_2, (b) TiO_2-rGO (0.05 wt%), (c) TiO_2-rGO (1 wt%), and (d) TiO_2-rGO (5 wt%);.

To investigate the enhanced photocatalytic mechanism of the TiO_2-rGO composite, the adsorption ability for the phenol solution of the TiO_2-rGO composite was investigated, as shown in Fig. 8C. It is clear that the adsorption ability for phenol is greatly improved with increasing amount of rGO in the TiO_2-rGO composite. Since the photocatalytic decomposition of organic substances takes place on the surface of a photocatalyst, the enrichment of the organic substances close to the photocatalysts is an important contributing factor for achieving higher photocatalytic performance [13,51]. In this study, phenol molecules in the solution can transfer from the solution to the photocatalyst surface and be adsorbed on the surface of graphene via π–π conjugation between phenol and aromatic regions of graphene [43,52].

Fig. 9 shows the possible photocatalytic mechanism of the TiO_2-rGO composites. Under UV-light irradiation, the photogenerated electrons on the conduction band of TiO_2 can effectively reduce oxygen via the rGO nanosheets. In this case, the rGO nanosheets

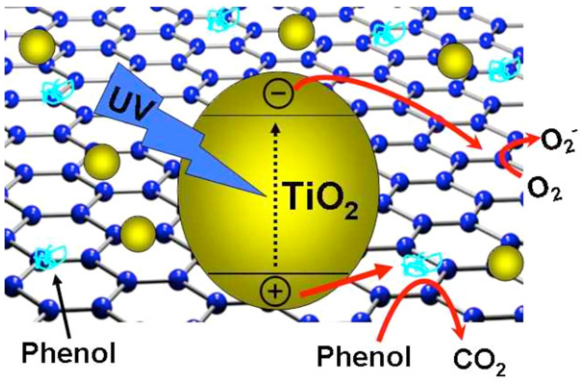

Fig. 9. Schematic diagram for illuminating the charge behavior at the interface of TiO_2 and rGO.

work as a cocatalyst for the rapid transfer of photogenerated electrons from the TiO_2, resulting in a lower recombination rate and enhanced photocatalytic activity [13]. In fact, the rapid transfer mechanism of photogenerated electrons for the improved photocatalytic performance in this study is similar to the well-known noble metal-modified semiconductor photocatalysts, where the noble metal functions as an electron sink to accept photogenerated electrons from excited semiconductor facilitating oxygen reduction [6,7]. On the other hand, considering the enrichment of phenol molecules on the surface of rGO nanosheets from the solution and the strong coupling of TiO_2 nanoparticles and rGO, it is believed the photogenerated holes on the valence band of TiO_2 can easily transfer to the phenol molecules on the rGO surface via holes or •OH, resulting in a rapid decomposition. In addition, when the phenol molecules adsorbed on the surface of TiO_2 are decomposited, it is possible that the enriched phenol molecules on the rGO surface can diffuse onto the active sites of TiO_2 for the further decomposition. Therefore, it is clear that the effective separation and high-efficiency utilization of photogenerated electrons and holes contribute to an obviously enhanced photocatalytic performance of the TiO_2-rGO composite photocatalysts.

Compared with the commercial powdered photocatalysts, the present suspensible TiO_2-rGO composite photocatalysts have more advantages. As a good photocatalyst for practical applications in wastewater, the photocatalysts should be easily reclaimed and re-used in addition to its high efficiency. It is clear that P25 photocatalyst almost cannot be separated completely from a slurry system after photocatalytic reaction owing to its small particle size, although it usually shows a high photocatalytic performance. In this study, it is found that the prepared TiO_2-rGO composite photocatalysts show a cotton-like structure, as shown in Fig. 1. Therefore, the suspensible TiO_2-rGO composite photocatalysts can be easily separated from the aqueous solution after photocatalytic reaction and then re-dispersed into the solution for the further application. Considering the facile and completely green preparation without the use any additives or surfactants, the present easy-recycling TiO_2-rGO composite photocatalysts can be regarded as one of the ideal and novel photocatalysts for the application at industrial scales, which has been seriously impeded by the high cost for separating nanocrystal catalysts.

4. Conclusions

The easily recycled TiO_2-rGO composite were prepared by a one-step green hydrothermal method without using any additive and surfactant. The one-step formation mechanism of the TiO_2-rGO composites is based on the initial formation of strong-coupling TiO_2-GO nanocomposite and the subsequent in situ reduction of GO to rGO during hydrothermal treatment. The TiO_2 nanoparticles with a clean surface and a good dispersion are highly required for the formation of the easy-recycling TiO_2-rGO composites. Compared with the high-efficiency P25 TiO_2 precursor, the photocatalytic performance can be obviously improved (about 23%) for the decomposition of phenol after coupling 1-wt% rGO. The enhanced photocatalytic performance can be attributed the cooperation effect of the effective separation of charge carriers via rGO cocatalyst, the enrichment of phenol molecular on the rGO, and the strong coupling interaction between TiO_2 nanoparticles and rGO nanosheets. Considering the facile and completely green preparation of the TiO_2-rGO composite photocatalysts, this work may provide some insight into the design of other novel graphene-based materials, and the present recoverable TiO_2-rGO composite photocatalysts can be regards as one of the ideal photocatalysts for the various potential applications.

Acknowledgments

This work was partially supported by the National Natural Science Foundation of China (21277017, 61274129, 51208396 and 51272031), 973 Program (2013CB632402, 2010CB923200) and 863 Program (2012AA062701). This work was also financially supported by the Fundamental Research Funds for the Central Universities (Grants 2011-Ia-039, 2011-Ia-016).

References

[1] M.R. Hoffmann, S.T. Martin, W. Choi, D.W. Bahnemann, Chemical Reviews 95 (1995) 69–96.
[2] K.L. Lv, B. Cheng, J.G. Yu, G. Liu, Physical Chemistry Chemical Physics 14 (2012) 5349–5362.
[3] S.W. Liu, J.G. Yu, B. Cheng, M. Jaroniec, Advances in Colloid and Interface Science 173 (2012) 35–53.
[4] Z.F. Liu, Z.G. Zhao, M. Miyauchi, Journal of Physical Chemistry C 113 (2009) 17132–17137.
[5] X.F. Wang, S.F. Li, Y.Q. Ma, H.G. Yu, J.G. Yu, Journal of Physical Chemistry C 115 (2011) 14648–14655.
[6] J.G. Yu, J.F. Xiong, B. Cheng, S.W. Liu, Applied Catalysis B: Environmental 60 (2005) 211–221.
[7] I.M. Arabatzis, T. Stergiopoulos, M.C. Bernard, D. Labou, S.G. Neophytides, P. Falaras, Applied Catalysis B: Environmental 42 (2003) 187–201.
[8] H. Yu, H. Irie, Y. Shimodaira, Y. Hosogi, Y. Kuroda, M. Miyauchi, K. Hashimoto, Journal of Physical Chemistry C 114 (2010) 16481–16487.
[9] H. Yu, H. Irie, K. Hashimoto, Journal of the American Chemical Society 132 (2010) 6898–6899.
[10] X.Z. Li, F.B. Li, C.L. Yang, W.K. Ge, Journal of Photochemistry and Photobiology A: Chemistry 141 (2001) 209–217.
[11] Z.H. Xu, J.G. Yu, Nanoscale 3 (2011) 3138–3144.
[12] Q.J. Xiang, J.G. Yu, M. Jaroniec, Chemical Society Reviews 41 (2012) 782–796.
[13] W.G. Wang, J.G. Yu, Q.J. Xiang, B. Cheng, Applied Catalysis B: Environmental 119 (2012) 109–116.
[14] S.W. Liu, C. Liu, W.G. Wang, B. Cheng, J.G. Yu, Nanoscale 4 (2012) 3193–3200.
[15] Y. Wang, R. Shi, J. Lin, Y. Zhu, Applied Catalysis B: Environmental 100 (2010) 179–183.
[16] G. Williams, B. Seger, P.V. Kamat, ACS Nano 2 (2008) 1487–1491.
[17] W. Gao, L.B. Alemany, L.J. Ci, P.M. Ajayan, Nature Chemistry 1 (2009) 403–408.
[18] S. Park, R.S. Ruoff, Nature Nanotechnology 4 (2009) 217–224.
[19] S. Stankovich, D.A. Dikin, R.D. Piner, K.A. Kohlhaas, A. Kleinhammes, Y. Jia, Y. Wu, S.T. Nguyen, R.S. Ruoff, Carbon 45 (2007) 1558–1565.
[20] Y. Si, E.T. Samulski, Nano Letters 8 (2008) 1679–1682.
[21] Y. Ding, P. Zhang, Q. Zhuo, H. Ren, Z. Yang, Y. Jiang, Nanotechnology 22 (2011) 215601.
[22] J. Liu, H. Bai, Y. Wang, Z. Liu, X. Zhang, D.D. Sun, Advanced Functional Materials 20 (2010) 4175–4181.
[23] X.Y. Zhang, H.P. Li, X.L. Cui, Y.H. Lin, Journal of Materials Chemistry 20 (2010) 2801–2806.
[24] D.H. Wang, D.W. Choi, J. Li, Z.G. Yang, Z.M. Nie, R. Kou, D.H. Hu, C.M. Wang, L.V. Saraf, J.G. Zhang, I.A. Aksay, J. Liu, ACS Nano 3 (2009) 907–914.
[25] T.N. Lambert, C.A. Chavez, B. Hernandez-Sanchez, P. Lu, N.S. Bell, A. Ambrosini, T. Friedman, T.J. Boyle, D.R. Wheeler, D.L. Huber, Journal of Physical Chemistry C 113 (2009) 19812–19823.
[26] M.S.A. Sher Shah, A.R. Park, K. Zhang, J.H. Park, P.J. Yoo, ACS Applied Materials & Interfaces 4 (2012) 3893–3901.
[27] X.F. Wang, S.F. Li, H.G. Yu, J.G. Yu, Journal of Molecular Catalysis A: Chemical 334 (2011) 52–59.

[28] H.G. Yu, S.C. Lee, J.G. Yu, C.H. Ao, Journal of Molecular Catalysis A: Chemical 246 (2006) 206–211.
[29] Y. Xu, H. Bai, G. Lu, C. Li, G. Shi, Journal of the American Chemical Society 130 (2008) 5856–5857.
[30] R. Liu, P. Wang, X. Wang, H. Yu, J. Yu, Journal of Physical Chemistry C 116 (2012) 17721–17728.
[31] H.G. Yu, L. Liu, X.F. Wang, P. Wang, J.G. Yu, Y.H. Wang, Dalton Transactions 41 (2012) 10405–10411.
[32] H.G. Yu, R. Liu, X.F. Wang, P. Wang, J.G. Yu, Applied Catalysis B: Environmental 111 (2012) 326–333.
[33] X.F. Wang, S.F. Li, H.G. Yu, J.G. Yu, S.W. Liu, Chemistry – A European Journal 17 (2011) 7777–7780.
[34] C. Nethravathi, M. Rajamathi, Carbon 46 (2008) 1994–1998.
[35] W.Q. Fan, Q.H. Lai, Q.H. Zhang, Y. Wang, Journal of Physical Chemistry C 115 (2011) 10694–10701.
[36] B.Y. Xia, H.B. Wu, J.S. Chen, Z.Y. Wang, X. Wang, X.W. Lou, Physical Chemistry Chemical Physics 14 (2012) 473–476.
[37] L. Ren, X. Qi, Y.D. Liu, Z.Y. Huang, X.L. Wei, J. Li, L.W. Yang, J.X. Zhong, Journal of Materials Chemistry 22 (2012) 11765–11771.
[38] H.J. Song, L.C. Zhang, C.L. He, Y. Qu, Y.F. Tian, Y. Lv, Journal of Materials Chemistry 21 (2011) 5972–5977.
[39] Y. Zhou, Q. Bao, L.A.L. Tang, Y. Zhong, K.P. Loh, Chemistry of Materials 21 (2009) 2950–2956.
[40] X.M. Sun, Y.D. Li, Angewandte Chemie International Edition 43 (2004) 597–601.
[41] C.H. Yao, Y.S. Shin, L.Q. Wang, C.F. Windisch Jr., W.D. Samuels, B.W. Arey, C.M. Wang, W.M. Risen Jr., G.J. Exarhos, Journal of Physical Chemistry C 111 (2007) 15141–15145.
[42] J.G. Yu, H.G. Yu, B. Cheng, M.H. Zhou, X.J. Zhao, Journal of Molecular Catalysis A: Chemical 253 (2006) 112–118.
[43] S.D. Perera, R.G. Mariano, K. Vu, N. Nour, O. Seitz, Y. Chabal, K.J. Balkus, ACS Catalysis 2 (2012) 949–956.
[44] Q. Li, B.D. Guo, J.G. Yu, J.R. Ran, B.H. Zhang, H.J. Yan, J.R. Gong, Journal of the American Chemical Society 133 (2011) 10878–10884.
[45] J. Shen, T. Li, Y. Long, M. Shi, N. Li, M. Ye, Carbon 50 (2012) 2134–2140.
[46] J.G. Yu, H.G. Yu, B. Cheng, X.J. Zhao, J.C. Yu, W.K. Ho, Journal of Physical Chemistry B 107 (2003) 13871–13879.
[47] Q.J. Xiang, J.G. Yu, M. Jaroniec, Journal of the American Chemical Society 134 (2012) 6575–6578.
[48] D.C. Luo, G.X. Zhang, J.F. Liu, X.M. Sun, Journal of Physical Chemistry C 115 (2011) 11327–11335.
[49] H.L. Wang, J.T. Robinson, X.L. Li, H.J. Dai, Journal of the American Chemical Society 131 (2009) 9910–9911.
[50] O. Akhavan, M. Abdolahad, A. Esfandiar, M. Mohatashamifar, Journal of Physical Chemistry C 114 (2010) 12955–12959.
[51] Y. Zhang, Z.-R. Tang, X. Fu, Y.-J. Xu, ACS Nano 4 (2010) 7303–7314.
[52] H. Zhang, X. Lv, Y. Li, Y. Wang, J. Li, ACS Nano 4 (2009) 380–386.
[53] F. Wang, K. Zhang, Journal of Molecular Catalysis A: Chemical 345 (2011) 101–107.